PLOS ONE

RESEARCH ARTICLE

Normalized Neural Representations of Complex Odors

David Zwicker[1,2]*

1 School of Engineering and Applied Sciences, Harvard University, Cambridge, MA 02138, United States of America, **2** Kavli Institute for Bionano Science and Technology, Harvard University, Cambridge, MA 02138, United States of America

* dzwicker@seas.harvard.edu

Citation: Zwicker D (2016) Normalized Neural Representations of Complex Odors. PLoS ONE 11(11): e0166456. doi:10.1371/journal.pone.0166456

Editor: Hiroaki Matsunami, Duke University, UNITED STATES

Received: August 18, 2016

Accepted: October 29, 2016

Published: November 11, 2016

Data Availability Statement: The python source code to run the simulations and produce the figures of this paper is available at https://github.com/david-zwicker/sensing-normalized-results.

Funding: This research was funded by the Simons Foundation (https://www.simonsfoundation.org/) and the German Science Foundation (www.dfg.de/en/) through ZW 222/1-1. The funders had no role in study design, data collection and analysis, decision to publish, or preparation of the manuscript.

Competing Interests: The author has declared that no competing interests exist.

Abstract

The olfactory system removes correlations in natural odors using a network of inhibitory neurons in the olfactory bulb. It has been proposed that this network integrates the response from all olfactory receptors and inhibits them equally. However, how such global inhibition influences the neural representations of odors is unclear. Here, we study a simple statistical model of the processing in the olfactory bulb, which leads to concentration-invariant, sparse representations of the odor composition. We show that the inhibition strength can be tuned to obtain sparse representations that are still useful to discriminate odors that vary in relative concentration, size, and composition. The model reveals two generic consequences of global inhibition: (i) odors with many molecular species are more difficult to discriminate and (ii) receptor arrays with heterogeneous sensitivities perform badly. Comparing these predictions to experiments will help us to understand the role of global inhibition in shaping normalized odor representations in the olfactory bulb.

Introduction

Sensory systems encode information efficiently by removing redundancies present in natural stimuli [1, 2]. In natural images, for instance, neighboring regions are likely of similar brightness and the image can thus be characterized by the regions of brightness changes [3]. This structure is exploited by ganglion cells in the retina that respond to brightness gradients by receiving excitatory input from photo receptors in one location and inhibitory input from the surrounding [4]. This typical center-surround inhibition results in neural patterns that represent natural images efficiently [5]. Similarly, such local inhibition helps separating sound frequencies in the ear and locations touched on the skin [6]. Vision, hearing, and touch have in common that their stimulus spaces have a metric for which typical correlations in natural stimuli are local. Consequently, local inhibition can be used to remove these correlations and reduce the high-dimensional input to a lower-dimensional representation.

The olfactory stimulus space is also high-dimensional, since odors are comprised of many molecules at different concentrations. Moreover, the concentrations are also often correlated, e.g., because the molecules originate from the same source. However, these correlations are

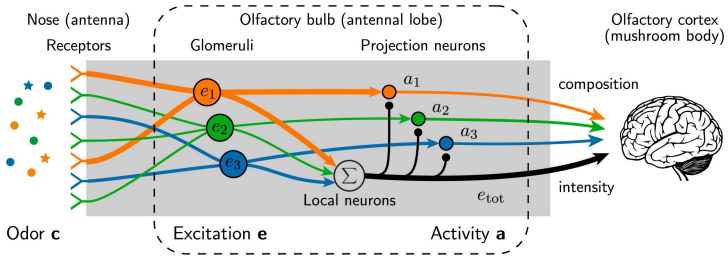

Fig 1. Schematic picture of our model describing the signal processing in the olfactory bulb. An odor comprised of many ligands excites the olfactory receptors and the signals from all receptors of the same type are accumulated in respective glomeruli. Associated projections neurons receive excitatory input from a single glomerulus and are subject to global inhibition, mediated by a network of local neurons. The activity of the projection neurons form a sparse, concentration-invariant odor representation.

doi:10.1371/journal.pone.0166456.g001

not represented by neighboring neurons in the olfactory system, since there is no obvious similarity metric for molecules that could be used to achieve such an arrangement [7]. Because the olfactory space lacks such a metric, local inhibition cannot be used to remove correlations to form an efficient representation [8–10]. Consequently, the experimentally discovered inhibition in the olfactory system [11] likely affects neurons irrespective of their location. Such global inhibition could for instance normalize the activities by their sum, which has been observed experimentally [12, 13]. This normalization cannot reduce the correlation structure of odors, but it could help separating the odor composition (what is present?) from the odor intensity (how much is there?) [14, 15]. This separation is useful, since the composition identifies an odor source, while the intensity information is necessary for finding or avoiding it. However, how global inhibition shapes such a bipartite representation of natural odors is little understood.

In this paper, we study a simple model of the olfactory system that resembles its first processing layers, which transform the odor representation successively [16, 17], see Fig 1. Our model connects previous results from simulations of the neural circuits [18–23] to system-level descriptions of the olfactory system [24–27]. To arrive at a general model of olfaction that applies to insects and mammals, we chose a simplified description, which focuses on global inhibition, as described in the next section. This global inhibition leads to normalization, which separates the odor composition from its intensity and encodes it in a sparse representation. The inhibition strength controls the trade-off between the sparsity and the transmitted information, which influences how well this code can be used to discriminate odors in typical olfactory tasks. The model reveals two generic consequences of global inhibition: (i) odors comprised of many different molecules exhibit sparser representations and should thus be more difficult to distinguish and (ii) overly sensitive receptors could dominate the sparse responses and arrays with heterogeneous receptors should thus perform poorly.

1 Simple Model of the Olfactory System

Odors are blends of odorant molecules that are ligands of the olfactory receptors. We describe an odor by a vector $\boldsymbol{c} = (c_1, c_2, \ldots, c_{N_L})$ that specifies the concentrations c_i of all N_L detectable ligands ($c_i \geq 0$). Generally, only a small subset of the $N_L \sim 10^5$ ligands are present in natural odors, so most of the c_i will typically be zero. The ligands in an odor are detected by olfactory receptor neurons, which reside in the nose in mammals and in the antenna in insects [28]. Each of these neurons expresses receptors of one of N_R genetically defined types, where $N_R \approx 50$ for flies [16], $N_R \approx 300$ for humans [29], and $N_R \approx 1000$ for mice [30]. The excitation

of all receptor neurons of the same type is accumulated in associated glomeruli [31], whose excitation pattern forms the first odor representation, see Fig 1. Here, the large number of ligands and their possible mixtures are represented by a combinatorial code, where each ligand typically excites multiple receptor types [32]. It has been shown experimentally that the excitation e_n of the glomerulus associated with receptor type n can be approximated by a linear function of the ligand concentrations $\boldsymbol{c}$ [33, 34],

$$e_n = \sum_{i=1}^{N_\mathrm{L}} S_{ni} c_i \ , \tag{1}$$

where S_{ni} denotes the sensitivity of glomerulus n to ligand i. We here consider a statistical description of combinatorial coding by studying random sensitivity matrices with entries drawn independently from a log-normal distribution. This distribution is parameterized by the mean sensitivity $\bar{S}$ and the standard deviation λ of the underlying normal distribution. This choice is motivated by experimental measurements, which also suggest that $\lambda \approx 1$ for flies and humans [27]. The random sensing implied by these sensitivities has been discussed in terms of compressed sensing [35, 36] and we showed previously that it typically decorrelates stimuli, thus leading to near-optimal odor representations on the level of glomeruli [27].

In contrast to our previous model, we here consider the odor representation encoded by projection neurons (mitral and tufted cells in mammals), which constitute the next layer after the glomeruli, see Fig 1. Projection neurons typically receive excitatory input from a single glomerulus [37] and inhibitory input from many local neurons (granule cells in mammals), which are connected to other projection neurons and glomeruli [15, 31]. The activity a_n of the projection neurons associated with receptor type n is a sigmoidal function of ligand concentrations, e.g., due to saturation of the receptors [38, 39]. Additionally, all signals are subject to noise, both from stochastic ligand-receptor interactions and from internal processing [40], which limits the number of distinguishable output activities. We capture both effects by considering the simple case where only two activities a_n can be distinguished. Here, the projection neurons are active when their excitatory input, the respective excitation e_n, exceeds a threshold γ,

$$a_n = \begin{cases} 0 & e_n \leq \gamma \\ 1 & e_n > \gamma \ . \end{cases} \tag{2}$$

Generally, γ could depend on the type n, but we here consider a simple mean-field model, where all types exhibit the same threshold. Nevertheless, this threshold could still depend on global variables. Experimental data [12, 13, 34, 41–45] and modeling of the local neurons [15, 22] suggest that the total excitation of all glomeruli inhibits all projection neurons. To capture this we postulate that the threshold γ is a function of the total excitation, where we for simplicity consider a linear dependence,

$$\gamma = \frac{\alpha}{N_\mathrm{R}} \sum_{n=1}^{N_\mathrm{R}} e_n \ . \tag{3}$$

Here, α is a parameter that controls the inhibition strength. In general, γ could be a non-linear function of the excitations, but the functional form cannot be inferred from current experimental data and we thus here consider the simple linear case to study how an adaptive threshold influences the odor representations.

Taken together, our model of the olfactory system comprises N_R communication channels, each consisting of receptors, a glomerulus, and projection neurons, which interact via global

inhibition, see Fig 1. The Eqs (1)–(3) describe how this system maps an odor $\boldsymbol{c}$ to an activity pattern $\boldsymbol{a} = (a_1, a_2, \ldots, a_{N_R})$. The amount of information that can be learned about $\boldsymbol{c}$ by observing $\boldsymbol{a}$ is quantified by the mutual information I, which reads

$$I = -\sum_{\boldsymbol{a}} P(\boldsymbol{a}) \log_2 P(\boldsymbol{a}) \ . \tag{4}$$

Here, the probability $P(\boldsymbol{a})$ of observing output $\boldsymbol{a}$ is given by $P(\mathbf{a}) = \int P(\mathbf{a}|\boldsymbol{c}) P_{\text{env}}(\boldsymbol{c})\, \mathrm{d}\boldsymbol{c}$. The conditional probability $P(\boldsymbol{a}|\boldsymbol{c})$ of observing $\boldsymbol{a}$ given $\boldsymbol{c}$ describes the processing in the olfactory system and follows from theEqs (1)–(3). In contrast, $P_{\text{env}}(\boldsymbol{c})$ denotes the probability of encountering an odor $\boldsymbol{c}$, which depends on the environment. Consequently, the information I is not only a function of the sensitivity matrix S_{ni} and the inhibition strength α, but also of the environment in which the receptors are used [27].

Natural odor statistics are hard to measure [46] and we thus cannot infer the distribution $P_{\text{env}}(\boldsymbol{c})$ from experimental data. Instead, we consider a broad class of distributions parameterized by a few parameters. For simplicity, we only consider uncorrelated odors, where the concentrations c_i of ligands are independent. We denote by p_i the probability that ligand i is part of an odor. If this is the case, the associated c_i is drawn from a log-normal distribution with mean μ_i and standard deviation σ_i. This choice allows us to independently adjust the mean mixture size $s = \sum_i p_i$, the mean of the total concentration $c_{\text{tot}} = \sum_i c_i$, and the concentration variations $\frac{\sigma_i}{\mu_i}$. Averaged over all odors, c_i then has mean $\langle c_i \rangle = p_i \mu_i$ and variance $\text{var}\,(c_i) = (p_i - p_i^2)\mu_i^2 + p_i \sigma_i^2$. Note that typical odors can have hundreds of different ligands [46], but this is still well below $N_L \sim 10^5$ and we thus have $1 \ll s \ll N_L$.

2 Results

2.1 Global inhibition leads to concentration-invariant, sparse representations

Our model has the interesting property that the odor representation $\boldsymbol{a}$ does not change when the odor $\boldsymbol{c}$ or the sensitivities S_{ni} are scaled by a positive factor. This is because both the excitations e_n and the threshold γ are linear in $\boldsymbol{c}$ and S_{ni}, see Eqs (1) and (3), and the activities a_n only depend on the ratio e_n/γ, see Eq (2). In fact, these equations can be interpreted as normalization of the excitations by the total excitation followed by thresholding with the constant threshold α/N_R. Since the representation $\boldsymbol{a}$ does not depend on c_{tot}, it only encodes relative ligand concentrations, i.e., the odor composition. This property is called concentration invariance and corresponds to the everyday experiences that odors smell the same over many orders of magnitude in concentration [23, 47, 48]. Indeed, experiments suggest that the activity of projection neurons is concentration-invariant [49, 50] and exhibits more uniform distances between odors [38, 50], indicating that they encode the odor composition efficiently.

To understand how odor compositions are encoded in our model, we start with numerical simulations of Eqs (1)–(3) as described in section A of the S1 Appendix. Fig 2A shows the excitations e_n corresponding to an arbitrary odor. Here, the excitation threshold is 1.4 times the mean excitation, and only three channels are active (orange bars). The corresponding histogram in Fig 2B shows that the number of active channels is typically small for this inhibition strength when odors are presented with statistics $P_{\text{env}}(\boldsymbol{c})$. Moreover, the magnitude of the Pearson correlation coefficient between two channels is typically only 1%, see section A of the S1 Appendix. This weak correlation is expected for the uncorrelated odors and random sensitivity matrices that we consider here and explains why the histogram in Fig 2B is close to a binomial

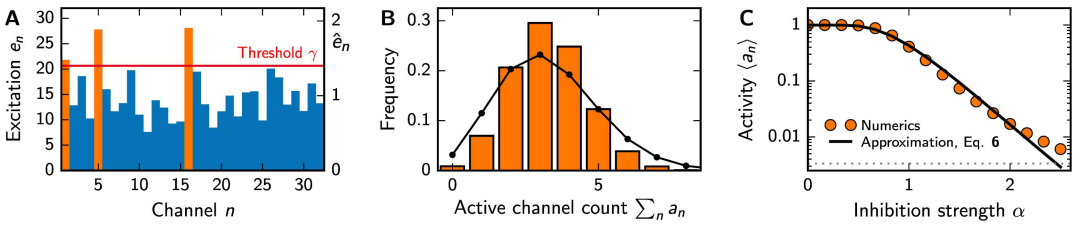

Fig 2. Global inhibition with thresholding leads to sparse odor representations *a*. (A) Excitations e_n for an arbitrary odor. Active channels (orange) have an excitation above the threshold (red line, inhibition strength $\alpha = 1.4$). The right axis indicates the normalized excitation $\hat{e}_n = e_n N_R / \sum_m e_m$. (B) Histogram of the number of active channels compared to a binomial distribution (black line) with the same mean for $\alpha = 1.4$. (C) Mean channel activity $\langle a_n \rangle$ as a function of α. The approximation given by Eq (6) (solid line) is compared to numerical simulations (symbols, standard error of the mean smaller than symbol size). The gray dotted line indicates a single expected active channel in humans, $\langle a_n \rangle = \frac{1}{300}$. (A–C) Additional model parameters are $N_R = 32$, $N_L = 256$, $p_i = 0.1$, $\mu_i = \sigma_i = 1$, and $\lambda = 1$.

doi:10.1371/journal.pone.0166456.g002

distribution. The odor representations are thus mainly characterized by the mean channel activity $\langle a_n \rangle$.

The mean channel activity $\langle a_n \rangle$ depends on the inhibition strength α, the sensitivities S_{ni}, and the odor statistics $P_{\text{env}}(\boldsymbol{c})$. To discuss these dependences, we next introduce an approximation based on a statistical description of the associated excitation e_n. Here, we define the normalized concentrations $\hat{c}_i = c_i / c_{\text{tot}}$ and normalized excitations $\hat{e}_n = e_n / (c_{\text{tot}} \bar{S})$, since a_n is independent of c_{tot} and $\bar{S}$. The statistics of $\hat{c}_i$ can be estimated in the typical case where odors are comprised of many ligands, see section B of the S1 Appendix. In the particular case where the ligands are identically distributed the mean is $\langle \hat{c}_i \rangle = N_L^{-1}$ and the variance reads $\text{var}(\hat{c}_i) \approx (1 - p + \sigma^2 \mu^{-2}) / (p N_L^2)$. Generally, $\hat{c}_i$ varies more if the underlying c_i has higher coefficient of variation σ_i / μ_i or if the mixture contains fewer ligands. The normalized excitation $\hat{e}_n$ is defined such that its mean is 1 and the associated variance can be written as a product of the external contribution $V_{\text{ext}} = \sum_i \langle \hat{c}_i^2 \rangle$ due to odors and the internal contribution $V_{\text{int}} = \text{var}(S_{ni}) \langle S_{ni} \rangle^{-2}$ due to sensitivities, see section B of the S1 Appendix. In the simple case of identically distributed ligands, we have

$$\text{var}(\hat{e}_n) = V_{\text{ext}} V_{\text{int}} \qquad V_{\text{ext}} \approx \frac{1}{s} \left(1 + \frac{\sigma^2}{\mu^2} \right) \qquad V_{\text{int}} = e^{\lambda^2} - 1 \,, \tag{5}$$

for $1 \ll s \ll N_L$, see section B of the S1 Appendix. The normalized excitations thus vary more if odors contain fewer ligands, concentrations fluctuate stronger, or sensitivities are distributed more broadly. Finally, the mean channel activity $\langle a_n \rangle$ is given by the probability that the excitation e_n exceeds the threshold γ, see Eq (2). This is equal to the probability that the normalized excitation $\hat{e}_n$ exceeds the normalized threshold $\hat{\gamma} = \gamma / (\bar{S} c_{\text{tot}})$. Replacing $\hat{\gamma}$ by its expectation value $\langle \hat{\gamma} \rangle = \alpha$ and using log-normally distributed e_n, we obtain

$$\langle a_n \rangle \approx \frac{1}{2} \,\text{erfc}\left(\frac{\zeta + \ln \alpha}{2 \zeta^{\frac{1}{2}}} \right) \qquad \text{with} \qquad \zeta = \frac{1}{2} \ln (1 + V_{\text{ext}} V_{\text{int}}) \,, \tag{6}$$

see section C of the S1 Appendix. Fig 2C shows that this is a good approximation of the numerical results, which have been obtained from ensemble averages of Eq (2). Note that $\langle a_n \rangle$ is independent of the dimensions N_L and N_R of the stimulus and the representation space, both in the approximation given in Eq (6) and for the numerical simulations, see Fig A in S1 Appendix. This is because we consider the simple case of uncorrelated odors and uncorrelated sensitivities.

The mean activity $\langle a_n \rangle$ can also be interpreted as the mean fraction of channels that are activated by an odor, such that small $\langle a_n \rangle$ corresponds to sparse odor representations. Fig 2C shows that in our model this is the case for large inhibition strength α, where $\langle a_n \rangle \sim e^{-\nu}$ with $\nu \approx (\ln \alpha)^2/(4\zeta)$, see section C of the S1 Appendix. Since sparse representations are thought to be efficient for further processing in the brain [14, 51] the inhibition strength α could be tuned, e.g., on evolutionary time scales, to achieve an activity $\langle a_n \rangle$ that is optimal for processing the odor representation downstream. If the optimal value of $\langle a_n \rangle$ is the same across animals, our theory predicts that inhibition is stronger in systems with more receptor types. However, this simple argument is not sufficient, since $\langle a_n \rangle$ also depends on the variations in the natural odor statistics and the receptor sensitivities, which determine V_{ext} and V_{int}, respectively. In particular, the width λ of the sensitivity distribution could also be under evolutionary control. However, experimental data suggests that both flies and humans exhibit $\lambda \approx 1$ [27]. Additionally, we show in Fig B of S1 Appendix that much smaller or larger values lead to extremely sparse representations, such that we will only consider $\lambda = 1$ in the following. In this case, the inhibition strength α controls the sparsity of the odor representation in our simple model of the olfactory system.

2.2 Sparse coding transmits useful information

One problem with sparse representations is that they cannot encode as many odors as dense representations. There is thus a maximal sparsity at which typical olfactory tasks can still be performed. In general, the performance of the olfactory system can be quantified by the transmitted information I, which is defined in Eq (4). If we for simplicity neglect the small correlations between channels, I can be approximated as [27]

$$I \approx -\sum_{n=1}^{N_{\text{R}}} \left[\langle a_n \rangle \log_2 \langle a_n \rangle + (1 - \langle a_n \rangle) \log_2 (1 - \langle a_n \rangle) \right] . \tag{7}$$

A maximum of N_{R} bits is transmitted when half the channels are active on average, $\langle a_n \rangle = \frac{1}{2}$. In our model, this is the case for weak inhibition, $\alpha \approx 1$, see Fig 2C. For significant inhibition, $\alpha > 1$, few channels are typically active and the transmitted information is smaller, see also Fig C in S1 Appendix. In the limit $\langle a_n \rangle \ll 1$, the information is approximately given by $I \sim \frac{1}{\ln 2} N_{\text{R}} \langle a_n \rangle \cdot (1 - \ln \langle a_n \rangle)$, which implies that even if only 10% of the channels are active on average, the information I is still almost half of the maximal value of N_{R} bits. However, large information I does not automatically indicate a good receptor array, since only accessible information that can be used to solve a given task matters [52, 53].

To test whether sparse representations are sufficient to solve typical olfactory tasks, we next study how well odors can be discriminated in our model. As a proxy for the discriminability, we calculate the Hamming distance d between the odor representations, which is given by the number of channels with different activity. In the simple case of unrelated odors, which have no ligands in common, the expected distance $\langle d \rangle$ is approximately given by the total number of active channels in both representations. Consequently, unrelated odors can be distinguished even if their representations are very sparse. However, realistic tasks typically require distinguishing similar odors. We thus next study the discriminability of odors that vary in the relative concentrations of their ligands, their size, and their composition.

We start by determining the maximal dilution $\frac{c_{\text{b}}}{c_{\text{t}}}$ at which a target odor at concentration c_{t} can still be detected in a background of concentration c_{b}. We calculate the expected difference $\langle d \rangle$ between the associated representations from the probability that a given channel changes its activity when the target is added, see section D of the S1 Appendix. Since this

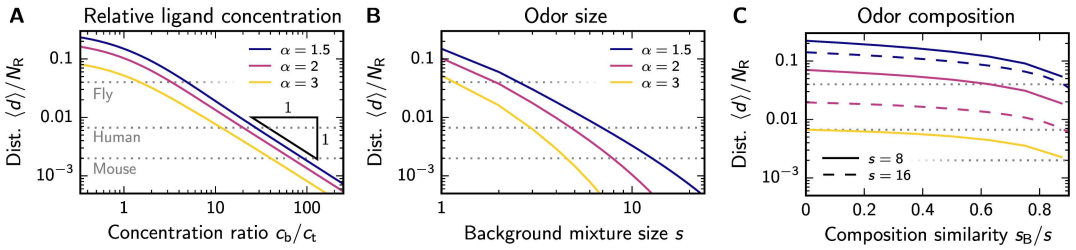

Fig 3. Sparse coding is sufficient to distinguish odors with different relative ligand concentrations, mixture size, and composition. (A) Mean distance $\langle d \rangle$ between the representations of a background ligand at concentration c_b and an odor with an additional target ligand at concentration c_t as a function of the dilution c_b/c_t for various inhibition strengths α. (B) Distance $\langle d \rangle$ resulting from adding a ligand to an odor comprised of s ligands as a function of s for various α. (C) Distance $\langle d \rangle$ between the representations of two odors with s ligands, sharing s_B of them, as a function of the similarity s_B/s for few ligands ($s = 8$, solid lines) and many ligands ($s = 16$, dashed lines). The colors indicate the same α as in the other panels. (A–C) The gray dotted lines indicate the threshold $\langle d \rangle = 2$ for $N_R = 50$, 300, 1000 (corresponding to flies, humans, and mice; top to bottom). The width of the sensitivity distribution is $\lambda = 1$.

doi:10.1371/journal.pone.0166456.g003

probability is the same for all channels, $\langle d \rangle$ is proportional to the number N_R of channels. For the simple case where both the target and the background are a single ligand, Fig 3A shows that $\langle d \rangle$ decreases for smaller target concentrations and is qualitatively the same for all inhibition strengths α. For large dilutions $\frac{c_b}{c_t}$, $\langle d \rangle$ is inversely proportional to the dilution, $\langle d \rangle \propto N_R \frac{c_t}{c_b}$. Since the addition of the target can only be detected reliably if $\langle d \rangle > 2$, which corresponds to a situation where one channel becomes inactive and another one active, our model predicts that doubling the number N_R of channels also doubles the concentration sensitivity. Fig 3A thus implies that mice ($N_R \approx 1000$) should be able to detect the addition of a target even if it is almost a hundred times more dilute than the background, which is close to the threshold that has been found experimentally [54]. Conversely, flies ($N_R \approx 50$) should fail for very small dilution factors.

We next study odors comprised of many ligands, since typical odors are blends [46]. For simplicity, we consider the detection of a single target ligand in a background mixture of varying size s when the target ligand and the ligands in the background have equal concentration, such that the target dilution is s. Fig 3B shows that the qualitative dependence of $\langle d \rangle$ on the dilution is similar to the single ligand case in panel A, but the maximal dilution for detecting the target is different. For instance, the model predicts that mice cannot identify the addition of the target ligand to a background consisting of more than ten ligands, while the maximal dilution was almost one hundred in the case of single background ligands. Consequently, the discrimination performance seems to drop significantly when larger mixtures are considered. This qualitatively agrees with experiments where humans are not able to identify all ligands in mixtures of more than three ligands [55, 56] and they fail to detect the presence or absence of ligands in mixtures of more then 15 ligands [57].

Even if humans cannot identify individual ligands in complex odors, they might still be able to distinguish two such odors. To study this, we next compare the representations of two odors that each contain s ligands, sharing s_B of them, for the simple case where all ligands have the same concentration. Fig 3C shows that the distance $\langle d \rangle$ between the two odors decreases with larger s_B, i.e., more similar odors are more difficult to discriminate. However, s_B only has a strong effect if more than about 80% of the ligands are shared between odors. Conversely, the inhibition strength α and the mixture size s significantly influence $\langle d \rangle$ for all values of s_B. This agrees with the results shown in Fig 3B, where $\langle d \rangle$ exhibits a similar dependence on α and s. While it is expected that the performance decreases with large inhibition strength α since fewer channels are active, the strong dependence on the size s is surprising.

2.3 Larger mixtures have sparser representations

Why are mixtures of many ligands more difficult to discriminate in our model? Since correlations between channels seem to be negligible, the most likely explanation is that larger mixtures activate fewer channels. To test this hypothesis, we determine the activity $\langle a_n \rangle$ in the simple case where all ligands in an odor have the same concentration. Because of the normalization, the value of this concentration does not matter and $\langle a_n \rangle$ only depends on the inhibition strength α and the mixture size s. In the limit of large mixtures ($s \gg 1$), the approximation given in Eq (6) yields $\langle a_n \rangle \sim e^{-\beta s}$ with $\beta \sim (\ln \alpha)^2$, see section C of the S1 Appendix. In this case, the activity $\langle a_n \rangle$ thus decreases exponentially with s and this decrease is stronger for larger α. Consequently, larger mixtures activate fewer channels and it is thus less likely that a small change in such odors alters the activation pattern $\boldsymbol{a}$.

Larger mixtures activate fewer channels because the respective excitations e_n have a smaller variability. For an odor with s ligands of equal concentration, e_n is proportional to the sum of s sensitivities S_{ni}, see Eq (1). Consequently, e_n can be considered as a random variable whose mean $\langle e_n \rangle$ and variance var(e_n) scale with s. The activity $\langle a_n \rangle$ is given by the fraction of excitations that exceed the threshold γ, which also scales with s. This fraction typically scales with the coefficient of variation $\mathrm{var}(e_n)^{\frac{1}{2}} \langle e_n \rangle^{-1}$, which is proportional to $s^{-\frac{1}{2}}$ and is thus smaller for larger mixtures. Larger mixtures thus activate fewer channels because there are fewer excitations that are much larger than the mean, see Fig 4A. This is a direct consequence of the assumption that the excitation threshold γ scales with the mean excitation and this result does not depend on other details of the model. Conversely, the dependence of $\langle a_n \rangle$ on the inhibition strength α is model specific, since it follows from the shape of the tail of the excitation distribution. In particular, the influence of the mixture size on $\langle a_n \rangle$ is insignificant for weak inhibition, $\alpha \approx 1$, because approximately half the channels are activated irrespective of the variance var (e_n).

This qualitative explanation illustrates that depending on the variability of the excitations different odors can have representations with very different sparsities. Indeed, we find that the sparsity changes over several orders of magnitude as a function of the mixture size s in our model, see Fig 4B. Moreover, the concentration variability $\frac{\sigma}{\mu}$ of the individual ligands also has a strong effect on the sparsity, see Fig 4C. This is because larger $\frac{\sigma}{\mu}$ implies larger variations in the excitations, such that more channels exceed the threshold and become active. In fact, this dependence of $\langle a_n \rangle$ on s and $\frac{\sigma}{\mu}$ is also qualitatively captured by the analytical approximation

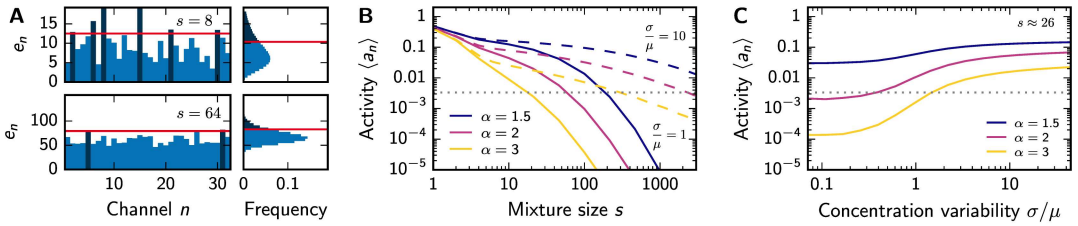

Fig 4. Larger mixtures activate fewer channels. (A) Comparison of the excitations e_n for odors with few ligands (mixture size $s = 8$, upper panels) and many ligands ($s = 64$, lower panels) at $\alpha = 1.3$. e_n for a single odor (left panels) and histograms for all odors (right panels) are shown. Larger mixtures exhibit fewer active channels (dark blue), for which the excitations are above threshold (red line). (B) Numerically determined $\langle a_n \rangle$ as a function of s for various inhibition strengths α at small ($\sigma/\mu = 1$, solid lines) and large concentration variability ($\sigma/\mu = 10$, dashed lines) at $N_L = 10^4$. (C) Numerically determined $\langle a_n \rangle$ as a function of σ/μ for various α. (A–C) Additional model parameters are $N_R = 32$, $N_L = 256$, $p_i = 0.1$, $\mu_i = \sigma_i = 1$, and $\lambda = 1$. The gray dotted line in B and C indicates a single expected active channel in humans, $\langle a_n \rangle = \frac{1}{300}$.

doi:10.1371/journal.pone.0166456.g004

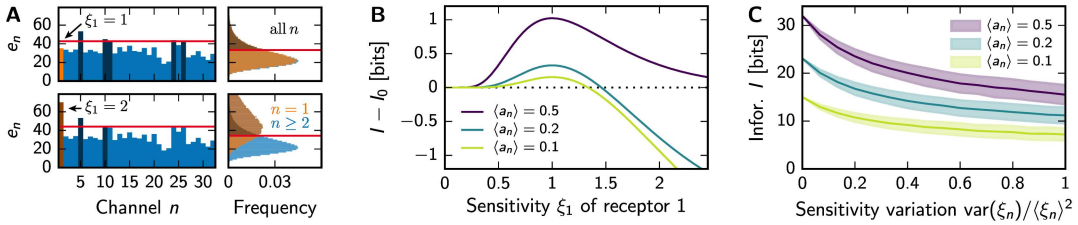

Fig 5. Receptors with diverse mean sensitivities make poor arrays. (A) Comparison of the excitations e_n for homogeneous ($\xi_1 = 1$, upper panels) and heterogeneous receptors ($\xi_1 = 2$, lower panels). e_n for the same arbitrary odor (left panels) and histograms for all odors (right panels) are shown for the first receptor ($n = 1$, orange) and all other receptors ($n \geq 2$, blue). Dark bars indicate excitations that are above the threshold (red line, inhibition strength $\alpha = 1.3$). (B) Information I given by Eq (7) as a function of the sensitivity ξ_1 of the first receptor. The channel activity $\langle a_n \rangle$ calculated from Eq (8) is set to the given value by adjusting α. I is shown relative to the information I_0 of a system without the first receptor (dotted line). (C) Information I (line, mean; shaded area indicates standard deviation) of log-normally distributed ξ_n as a function of the variation var$(\xi_n)\langle \xi_n \rangle^{-2}$ for various $\langle a_n \rangle$. (A–C) Remaining parameters are $N_R = 32$, $N_L = 256$, $p_i = 0.1$, $\mu_i = \sigma_i = 1$, and $\lambda = 1$.

doi:10.1371/journal.pone.0166456.g005

given in Eq (6), which explicitly depends on the odor variability V_{ext} defined in Eq (5). Taken together, our model shows that the sparsity of the odor representations strongly depend on the odor statistics $P_{env}(\boldsymbol{c})$.

2.4 Effective arrays have similar receptor sensitivities

So far, we considered homogeneous receptor arrays, where all receptor types have the same average sensitivity. However, receptors vary in their copy numbers [58], which implies different average sensitivities, see section E of the S1 Appendix. Additionally, point mutations of a receptor gene can change this receptor's sensitivities to almost all ligands [59]. Consequently, typical receptor arrays might be heterogeneous, where some receptor types have larger mean sensitivities than others. Such heterogeneous receptor arrays might be sub-optimal, since a channel with overly sensitive receptors will contribute significantly to the common threshold γ, suppress the activity of other channels, and could thus limit the coding capacity of the system, see Fig 5A.

We study heterogeneous receptor arrays by consider sensitivity matrices $S_{ni} = \xi_n S_{ni}^{iid}$, where ξ_n denotes the mean sensitivity of receptor type n and S_{ni}^{iid} is the sensitivity matrix that we discussed so far, i.e., it is a random matrix where all entries are independently drawn from a log-normal distribution described by the mean $\bar{S}$ and width λ. For this model, the mean excitation threshold is $\langle \gamma \rangle = \alpha \bar{S} \langle c_{tot} \rangle \xi_{tot} N_R^{-1}$ where $\xi_{tot} = \Sigma_n \xi_n$. The expected channel activity is approximately given by

$$\langle a_n \rangle \approx 1 - F\left(\frac{\alpha \xi_{tot}}{N_r \xi_n} \right) , \tag{8}$$

where $F(\hat{e}_n)$ is the cumulative distribution function of the normalized excitations $\hat{e}_n$ for $\xi_n = 1$, whose mean is $\langle \hat{e}_n \rangle = 1$ and whose variance is given by Eq (5). Note that $\langle a_n \rangle$ does not change if all ξ_n are multiplied by the same factor. In particular, the expression above reduces to $\langle a_n \rangle \approx 1 - F(\alpha)$ and thus Eq (6) if all ξ_n are equal.

We first discuss the influence of the receptor sensitivities ξ_n by only varying one type, i.e., we change ξ_1 while setting $\xi_n = 1$ for $n \geq 2$. Fig 5B shows that for fixed channel activity $\langle a_n \rangle$ the transmitted information I is maximal for a homogeneous receptor array ($\xi_1 = 1$). I is reduced for smaller ξ_1 and for $\xi_1 = 0$ it reaches the value I_0 of an array where the first receptor was removed. Conversely, I can drop well below I_0 when ξ_1 is increased above 1. In this case, the

large excitation of the affected channel not only leads to its likely activation, but it also raises the threshold γ and thereby inhibits other channels, see Fig 5A. In the extreme case of very large ξ_1, this channel will always be active while all other channels are silenced, which implies $I = 0$. There is thus a critical value of ξ_1 beyond which removing the receptor from the array is advantageous for the overall performance. Fig 5B shows that increasing the sensitivity of a receptor by only 40% can make it useless in the context of the whole array if representations are sparse.

So far, we only varied the sensitivity of a single receptor. To test how variations in the sensitivities of all receptors affect the information I, we next consider log-normally distributed ξ_n. Here, vanishing variance of ξ_n corresponds to a homogeneous receptor array. Fig 5C shows that small variations in ξ_n can strongly reduce the transmitted information I. Since I limits the discriminative capability of the receptor array, this suggests that receptor arrays with heterogeneous sensitivities perform worse.

This simple model shows that the excitation statistics of the different channels determine the properties of the resulting odor representation. In particular, receptors that have lower excitations on average might be suppressed often and thus contribute less to the odor information. Since the excitation statistics are influenced both by the sensitivities S_{ni} and the odor statistics $P_{\text{env}}(\boldsymbol{c})$, this suggests that the sensitivities should be adjusted to the odor statistics. In an optimal receptor array, the sensitivities are chosen such that all channels have the same probability to become active.

3 Discussion

We studied a simple model of odor representations, which is based on normalization and a non-linear gain function. This model separates the odor composition, encoded in the activity $\boldsymbol{a}$ of the projection neurons, from the odor intensity, which could be encoded by the total excitation e_{tot} or the threshold level γ [60]. For significant inhibition the representation $\boldsymbol{a}$ is sparse and the set of active projection neurons provides a natural odor 'tag' that could be used for identification and memorization in the downstream processing [35].

Sparse representations reduce the coding capacity and transmit less information than dense ones. However, even if the mean activity is $\langle a_n \rangle = 0.01$ and thus 50 times smaller than in maximally informative arrays with $\langle a_n \rangle = 0.5$, the transmitted information I is only reduced by a factor of 12, see Eq (7). For humans with $N_{\text{R}} = 300$, this yields $\boldsymbol{I} \approx 25$ bits, allowing to encode $2^I \approx 10^7$ different odor compositions. Note that the total information I_{tot} also includes information I_{int} about the odor intensity, $I_{\text{tot}} = I + I_{\text{int}}$. Here, $I_{\text{int}} \approx 10$ bits would be sufficient to encode the total concentration over a range of 10 orders of magnitude with a resolution of 5%, typical for humans [61]. In this case, our model compresses the 300 bits of a maximally informative representation on the level of glomeruli [27] to only $I_{\text{tot}} \approx 35$ bits on the level of projection neurons.

The model discussed here is similar to our previous model, where we discussed representations on the level of the glomeruli [27]. Both models use a maximum entropy principle to determine properties of optimal receptor arrays. To achieve this, the receptor sensitivities must be tailored to the odor statistics in both models. The main difference of the models is the global inhibition discussed here, which separates the odor composition from its intensity and thus removes the correlation between the glomeruli excitation and the odor intensity [62]. Consequently, odors can then be discriminated at all concentrations, while this was only possible in a narrow concentration range in the glomeruli model [27]. The additional normalization is thus useful to separate odors, even if the projection neurons encode less information than the respective glomeruli, see Fig C in S1 Appendix. To estimate this information, we consider

binary outputs in both models, which corresponds to very noisy channels. However, the glomeruli model discusses arrays of noisy receptor, while we here consider perfect receptors whose signal is first normalized and then subjected to noise. This additional processing reduces correlations and leads to sparse representations, which might simplify downstream computations. Consequently, this model is suitable for describing natural olfaction, where the capacity for the downstream computations is limited, while the glomeruli model is relevant for artificial olfaction [63], since computers have enough power to handle high-dimensional signals.

Sparse responses of projection neurons have been observed in experiments [39, 64, 65]. For instance, in mice 15% of the projection neurons respond to a given single ligand [13], suggesting significant inhibition. However, in locust about two third of the projection neurons respond to any given odor [66], which implies weak inhibition. It is thus conceivable that some animals exhibit sparse representations while others have maximally informative ones, although additional experiments are needed to characterize the representations better. A direct experiment could test whether the odor percept changes when the weakly responding glomeruli are disabled artificially. Additionally, it will be important to study the representations of mono-molecular odors and mixtures at various concentration to better resemble the natural odor statistics. For instance, our simple theory predicts that fewer than 15% of the projection neurons in mice respond when complex mixtures are presented. Indeed, experiments find that only 3 to 10% of the projection neurons in mice fire for complex urine odors [67]. Conversely, the statistics of the activity of projection neurons in flies seem to be independent of the stimulus [68].

Our theory can also be tested by measuring how well odors can be discriminated. For instance, psycho-physical experiments have shown that humans have difficulties to distinguish non-overlapping mixtures of more than ~ 30 intensity-matched components [69]. We can use this observation to estimate the inhibition strength α at which such mixtures excite few channels and are thus hardly discriminable in our model. Fig 4 shows that this is the case for $\alpha \approx 2$, where only channels whose excitation exceeds twice the mean would be active. Such strong inhibition would make it difficult to distinguish mixtures of many ligands, while small mixtures are easily distinguishable, similar to the experimental results [69]. Conversely, other experiments indicate that the mixture size only weakly influences the odor discriminability [70]. However, theses measurements are still consistent with an inhibition strength close to $\alpha \approx 2$, where only few channels have different activities when comparing two odors, see Fig 3C. If α would be much smaller, almost all mixtures could be distinguished perfectly, while a much larger α would make it difficult to distinguish any mixtures. Taken together, psycho-physical experiments suggest that there is significant inhibition, but there is conflicting evidence on whether the odor discriminability changes with mixture size.

The coding sparsity given by the mean channel activity $\langle a_n \rangle$ can be adjusted by changing the inhibition strength α or the width λ of the receptor sensitivity distribution in our model. Additionally, $\langle a_n \rangle$ is a function of the natural odor statistics, i.e., the typical number of ligands in odors and their concentration distribution. Consequently, α or λ must be adjusted to keep $\langle a_n \rangle$ constant if the odor statistics change, e.g., because of seasonal changes or migration to a different environment. This adjustment could happen on multiple timescales, reaching from evolutionary adaptations of the receptors to near-instantaneous adjustments of the involved neurons, and it is likely that the global inhibition is regulated on all levels [16]. In this paper, we investigated the simple case of constant α and λ, which corresponds to slow regulation, but it is conceivable that α could be regulated on short time scales. For instance, the threshold could be lowered for more complex odors to improve their discriminability. Our model

suggests that such additional mechanisms are necessary to efficiently discriminate odors of all sizes.

Our model also reveals that it is important to control the properties of the individual communication channels to have useful receptor arrays. For instance, increasing the sensitivity of a given receptor by 40% can be worse then removing it completely, see Fig 5A. Generally, a receptor array is only effective if the different channels have similar excitations on average. This suggests that the sensitivities are tightly controlled and maybe even adjusted to the odor statistics of the environment. On evolutionary time scales, the sensitivities could be regulated by point mutations of the receptors that change how ligands bind [59]. On shorter time scales, the sensitivities could be regulated by changing the receptor copy numbers, see section E of the S1 Appendix. Since this is observed experimentally [58], we predict that the receptor copy numbers are adjusted such that the excitations of all glomeruli are similar when averaged over natural odors. Alternatively, variations in the receptor sensitivities could be balanced by more complex inhibition mechanism. For instance, experiments show that different projection neurons have different susceptibilities to inhibition [43]. Here, the experimentally observed turnover of mitral/granule cells and interneurons [71] could adjust the inhibition mechanism locally, which could optimize the olfactory system for a given environment [54]. Such adaptation of the inhibition mechanism to the current stimulus statistics and more complex models where the behavioral state of an animal could influence the olfactory bulb by top-down modulation [16] will be interesting to explorer in the future.

Our simplified model neglects many details of the olfactory system [17]. For instance, we do not consider the dynamics of inhalation and the odor absorption in the mucus [72, 73]. Instead, we here directly parameterize the ligand distribution at the olfactory receptors, where we for simplicity neglect correlations between ligands. It would be interesting to extend the model for more complex stimuli and study how the system decorrelates the input, identifies a target odor in a background, and separates multiple odors from each other. This likely involves many steps [48] and cannot be done perfectly with a single normalization step and non-linear gain function. For instance, it might be important to apply gain functions at the level of receptors and the glomeruli to model finite sensitivity and saturation effects [74]. Additionally, it has been shown that there is additional cross-talk on the level of receptors [75] and glomeruli [34, 41], which could support decorrelation. Generally, such cross-talk and the inhibition that we discussed here will be non-linear [76, 77]. This could for instance be modeled by a divisive normalization model that has been proposed for olfaction [12]. It is also likely that the inhibition of the projection neurons is not driven by a single global variable. If glomeruli positioning carried some meaning [9], local inhibition could help separating similar odors by enhancing the contrast [78]. The discrimination of similar odors could also be improved if projection neurons had a larger output range, increasing the information capacity per channel. Additionally, the two classes of projection neurons in mammals (mitral and tufted cells) exhibit different inhibition dynamics and might thus act as parallel communication channels [79]. Finally, we completely neglected the temporal dynamics of the olfactory system, which play an important role for the adaptation between sniffs [80] and might also influence odor perception within a single sniff [81–84].

Supporting Information

S1 Appendix. Supplementary material.
(PDF)

Acknowledgments

I thank Michael P. Brenner, Alexander T. Mathis, Venkatesh N. Murthy, Mikhail Tikhonov, and Christoph A. Weber for helpful discussions and comments on the manuscript. This research was funded by the Simons Foundation and the German Science Foundation through ZW 222/1-1.

Author Contributions

Conceptualization: DZ.

Data curation: DZ.

Formal analysis: DZ.

Investigation: DZ.

Funding acquisition: DZ.

Methodology: DZ.

Project administration: DZ.

Software: DZ.

Validation: DZ.

Visualization: DZ.

Writing – original draft: DZ.

Writing – review & editing: DZ.

References

1. Barlow HB. Possible principles underlying the transformations of sensory messages. In: Rosenblith WA, editor. Sensory Communication. MIT press; 1961. p. 217–234.
2. Barlow H. Redundancy reduction revisited. Network. 2001; 12(3):241–53. doi: 10.1080/net.12.3.241.253 PMID: 11563528
3. Ruderman, Bialek. Statistics of natural images: Scaling in the woods. Phys Rev Lett. 1994; 73(6): 814–817. doi: 10.1103/PhysRevLett.73.814 PMID: 10057546
4. Demb JB, Singer JH. Functional circuitry of the retina. Annual Review of Vision Science. 2015; 1: 263–289. doi: 10.1146/annurev-vision-082114-035334
5. Carandini M, Heeger DJ. Normalization as a canonical neural computation. Nat Rev Neurosci. 2012; 13(1):51–62.
6. Isaacson JS, Scanziani M. How inhibition shapes cortical activity. Neuron. 2011; 72(2):231–43. doi: 10.1016/j.neuron.2011.09.027 PMID: 22017986
7. Nikolova N, Jaworska J. Approaches to measure chemical similarity–a review. QSAR & Combinatorial Science. 2003; 22(9–10):1006–1026. doi: 10.1002/qsar.200330831
8. Soucy ER, Albeanu DF, Fantana AL, Murthy VN, Meister M. Precision and diversity in an odor map on the olfactory bulb. Nat Neurosci. 2009; 12(2):210–220. doi: 10.1038/nn.2262 PMID: 19151709
9. Murthy VN. Olfactory maps in the brain. Annu Rev Neurosci. 2011; 34:233–258. doi: 10.1146/annurev-neuro-061010-113738 PMID: 21692659
10. Urban NN. Lateral inhibition in the olfactory bulb and in olfaction. Physiol Behav. 2002; 77(4–5):607–12. doi: 10.1016/S0031-9384(02)00895-8 PMID: 12527007
11. Yokoi M, Mori K, Nakanishi S. Refinement of odor molecule tuning by dendrodendritic synaptic inhibition in the olfactory bulb. Proc Natl Acad Sci USA. 1995; 92(8):3371–5. doi: 10.1073/pnas.92.8.3371 PMID: 7724568
12. Olsen SR, Bhandawat V, Wilson RI. Divisive normalization in olfactory population codes. Neuron. 2010; 66(2):287–99. doi: 10.1016/j.neuron.2010.04.009 PMID: 20435004

13. Roland B, Jordan R, Sosulski DL, Diodato A, Fukunaga I, Wickersham I, et al. Massive normalization of olfactory bulb output in mice with a 'monoclonal nose'. Elife. 2016; 5. doi: 10.7554/eLife.16335 PMID: 27177421
14. Laurent G. A systems perspective on early olfactory coding. Science. 1999; 286(5440):723–8. doi: 10.1126/science.286.5440.723 PMID: 10531051
15. Cleland TA. Early transformations in odor representation. Trends Neurosci. 2010; 33(3):130–139. doi: 10.1016/j.tins.2009.12.004 PMID: 20060600
16. Wilson RI. Early olfactory processing in Drosophila: mechanisms and principles. Annu Rev Neurosci. 2013; 36:217–41. doi: 10.1146/annurev-neuro-062111-150533 PMID: 23841839
17. Silva Teixeira CS, Cerqueira NMFSA, Silva Ferreira AC. Unravelling the Olfactory Sense: From the Gene to Odor Perception. Chem Senses. 2016; 41(2):105–21. PMID: 26688501
18. Li Z. A model of olfactory adaptation and sensitivity enhancement in the olfactory bulb. Biol Cybern. 1990; 62(4):349–61. doi: 10.1007/BF00201449 PMID: 2310788
19. Li Z. Modeling the sensory computations of the olfactory bulb. In: Models of neural networks. Springer; 1994. p. 221–251. doi: 10.1007/978-1-4612-4320-5_6
20. Linster C, Hasselmo M. Modulation of inhibition in a model of olfactory bulb reduces overlap in the neural representation of olfactory stimuli. Behavioural brain research. 1997; 84(1):117–127. doi: 10.1016/S0166-4328(97)83331-1 PMID: 9079778
21. Getz WM, Lutz A. A neural network model of general olfactory coding in the insect antennal lobe. Chem Senses. 1999; 24(4):351–72. doi: 10.1093/chemse/24.4.351 PMID: 10480672
22. Cleland TA, Sethupathy P. Non-topographical contrast enhancement in the olfactory bulb. BMC Neurosci. 2006; 7:7. doi: 10.1186/1471-2202-7-7 PMID: 16433921
23. Zhang D, Li Y, Wu S. Concentration-invariant odor representation in the olfactory system by presynaptic inhibition. Comput Math Methods Med. 2013; 2013:507143. doi: 10.1155/2013/507143 PMID: 23533540
24. Hainer R, Emslie A, Jacobson A. An information theory of olfaction. Annals of the New York Academy of Sciences. 1954; 58(2):158–174. doi: 10.1111/j.1749-6632.1954.tb54851.x PMID: 13139345
25. Hopfield J. Odor space and olfactory processing: collective algorithms and neural implementation. Proc Natl Acad Sci USA. 1999; 96(22):12506–12511. doi: 10.1073/pnas.96.22.12506 PMID: 10535952
26. Koulakov A, Gelperin A, Rinberg D. Olfactory coding with all-or-nothing glomeruli. J Neurophysiol. 2007; 98(6):3134–3142. doi: 10.1152/jn.00560.2007 PMID: 17855585
27. Zwicker D, Murugan A, Brenner MP. Receptor arrays optimized for natural odor statistics. Proc Natl Acad Sci USA. 2016; 113(20):5570–75. doi: 10.1073/pnas.1600357113 PMID: 27102871
28. Kaupp UB. Olfactory signalling in vertebrates and insects: differences and commonalities. Nat Rev Neurosci. 2010; 11(3):188–200. doi: 10.1038/nrn2789 PMID: 20145624
29. Verbeurgt C, Wilkin F, Tarabichi M, Gregoire F, Dumont JE, Chatelain P. Profiling of olfactory receptor gene expression in whole human olfactory mucosa. PLOS ONE. 2014; 9(5):e96333. doi: 10.1371/journal.pone.0096333 PMID: 24800820
30. Niimura Y. Olfactory receptor multigene family in vertebrates: from the viewpoint of evolutionary genomics. Curr Genomics. 2012; 13(2):103–14. doi: 10.2174/138920212799860706 PMID: 23024602
31. Su CY, Menuz K, Carlson JR. Olfactory perception: receptors, cells, and circuits. Cell. 2009; 139(1):45–59. doi: 10.1016/j.cell.2009.09.015 PMID: 19804753
32. Malnic B, Hirono J, Sato T, Buck LB. Combinatorial receptor codes for odors. Cell. 1999; 96(5):713–723. doi: 10.1016/S0092-8674(00)80581-4 PMID: 10089886
33. Tabor R, Yaksi E, Weislogel JM, Friedrich RW. Processing of odor mixtures in the zebrafish olfactory bulb. J Neurosci. 2004; 24(29):6611–20. doi: 10.1523/JNEUROSCI.1834-04.2004 PMID: 15269273
34. Silbering AF, Galizia CG. Processing of odor mixtures in the Drosophila antennal lobe reveals both global inhibition and glomerulus-specific interactions. J Neurosci. 2007; 27(44):11966–77. doi: 10.1523/JNEUROSCI.3099-07.2007 PMID: 17978037
35. Stevens CF. What the fly's nose tells the fly's brain. Proc Natl Acad Sci USA. 2015; 112(30):9460–5. doi: 10.1073/pnas.1510103112 PMID: 26150492
36. Ganguli S, Sompolinsky H. Compressed sensing, sparsity, and dimensionality in neuronal information processing and data analysis. Annu Rev Neurosci. 2012; 35:485–508. doi: 10.1146/annurev-neuro-062111-150410 PMID: 22483042
37. Jefferis GS, Marin EC, Stocker RF, Luo L. Target neuron prespecification in the olfactory map of Drosophila. Nature. 2001; 414(6860):204–8. doi: 10.1038/35102574 PMID: 11719930

38. Bhandawat V, Olsen SR, Gouwens NW, Schlief ML, Wilson RI. Sensory processing in the Drosophila antennal lobe increases reliability and separability of ensemble odor representations. Nat Neurosci. 2007; 10(11):1474–82. doi: 10.1038/nn1976 PMID: 17922008

39. Tan J, Savigner A, Ma M, Luo M. Odor information processing by the olfactory bulb analyzed in gene-targeted mice. Neuron. 2010; 65(6):912–26. doi: 10.1016/j.neuron.2010.02.011 PMID: 20346765

40. Lowe G, Gold GH. Olfactory transduction is intrinsically noisy. Proc Natl Acad Sci USA. 1995; 92(17): 7864–8. doi: 10.1073/pnas.92.17.7864 PMID: 7544007

41. Aungst JL, Heyward PM, Puche AC, Karnup SV, Hayar A, Szabo G, et al. Centre-surround inhibition among olfactory bulb glomeruli. Nature. 2003; 426(6967):623–9. doi: 10.1038/nature02185 PMID: 14668854

42. Asahina K, Louis M, Piccinotti S, Vosshall LB. A circuit supporting concentration-invariant odor perception in Drosophila. J Biol. 2009; 8(1):9. doi: 10.1186/jbiol108 PMID: 19171076

43. Hong EJ, Wilson RI. Simultaneous encoding of odors by channels with diverse sensitivity to inhibition. Neuron. 2015; 85(3):573–89. doi: 10.1016/j.neuron.2014.12.040 PMID: 25619655

44. Banerjee A, Marbach F, Anselmi F, Koh MS, Davis MB, Garcia da Silva P, et al. An Interglomerular Circuit Gates Glomerular Output and Implements Gain Control in the Mouse Olfactory Bulb. Neuron. 2015; 87(1):193–207. doi: 10.1016/j.neuron.2015.06.019 PMID: 26139373

45. Berck ME, Khandelwal A, Claus L, Hernandez-Nunez L, Si G, Tabone CJ, et al. The wiring diagram of a glomerular olfactory system. Elife. 2016; 5. doi: 10.7554/eLife.14859 PMID: 27177418

46. Wright GA, Thomson MG. Odor Perception and the Variability in Natural Odor Scenes. In: Romeo J, editor. Integrative Plant Biochemistry. vol. 39 of Recent Advances in Phytochemistry. Elsevier; 2005. p. 191–226. doi: 10.1016/S0079-9920(05)80009-7

47. Uchida N, Mainen ZF. Odor concentration invariance by chemical ratio coding. Front Syst Neurosci. 2007; 1:3. doi: 10.3389/neuro.06.003.2007 PMID: 18958244

48. Cleland TA, Chen SYT, Hozer KW, Ukatu HN, Wong KJ, Zheng F. Sequential mechanisms underlying concentration invariance in biological olfaction. Front Neuroeng. 2011; 4:21. doi: 10.3389/fneng.2011.00021 PMID: 22287949

49. Sachse S, Galizia CG. Role of inhibition for temporal and spatial odor representation in olfactory output neurons: a calcium imaging study. J Neurophysiol. 2002; 87(2):1106–17. PMID: 11826074

50. Cleland TA, Johnson BA, Leon M, Linster C. Relational representation in the olfactory system. Proc Natl Acad Sci USA. 2007; 104(6):1953–8. doi: 10.1073/pnas.0608564104 PMID: 17261800

51. Olshausen BA, Field DJ. Sparse coding of sensory inputs. Curr Opin Neurobiol. 2004; 14(4):481–7. doi: 10.1016/j.conb.2004.07.007 PMID: 15321069

52. Tikhonov M, Little SC, Gregor T. Only accessible information is useful: insights from gradient-mediated patterning. R Soc Open Sci. 2015; 2(11):150486. doi: 10.1098/rsos.150486 PMID: 26716005

53. Tkačik G, Bialek W. Information Processing in Living Systems. Annual Review of Condensed Matter Physics. 2016; 7(1):89–117. doi: 10.1146/annurev-conmatphys-031214-014803

54. Mouret A, Lepousez G, Gras J, Gabellec MM, Lledo PM. Turnover of newborn olfactory bulb neurons optimizes olfaction. J Neurosci. 2009; 29(39):12302–14. doi: 10.1523/JNEUROSCI.3383-09.2009 PMID: 19793989

55. Jinks A, Laing DG. The analysis of odor mixtures by humans: evidence for a configurational process. Physiol Behav. 2001; 72(1–2):51–63. doi: 10.1016/S0031-9384(00)00407-8 PMID: 11239981

56. Goyert HF, Frank ME, Gent JF, Hettinger TP. Characteristic component odors emerge from mixtures after selective adaptation. Brain Res Bull. 2007; 72(1):1–9. doi: 10.1016/j.brainresbull.2006.12.010 PMID: 17303501

57. Jinks A, Laing DG. A limit in the processing of components in odour mixtures. Perception. 1999; 28(3): 395–404. doi: 10.1068/p2898 PMID: 10615476

58. Yu CR, Wu Y. Regeneration and rewiring of rodent olfactory sensory neurons. Exp Neurol. 2016; doi: 10.1016/j.expneurol.2016.06.001 PMID: 27264358

59. Yu Y, Claire A, Ni MJ, Adipietro KA, Golebiowski J, Matsunami H, et al. Responsiveness of G protein-coupled odorant receptors is partially attributed to the activation mechanism. Proc Natl Acad Sci USA. 2015; 112(48):14966–14971. doi: 10.1073/pnas.1517510112 PMID: 26627247

60. Mainland JD, Lundström JN, Reisert J, Lowe G. From molecule to mind: an integrative perspective on odor intensity. Trends Neurosci. 2014; 37(8):443–454. doi: 10.1016/j.tins.2014.05.005 PMID: 24950600

61. Cain WS. Differential sensitivity for smell: "Noise" at the nose. Science. 1977; 195(4280):796–798. doi: 10.1126/science.836592 PMID: 836592

62. Haddad R, Weiss T, Khan R, Nadler B, Mandairon N, Bensafi M, et al. Global features of neural activity in the olfactory system form a parallel code that predicts olfactory behavior and perception. J Neurosci. 2010; 30(27):9017–26. doi: 10.1523/JNEUROSCI.0398-10.2010 PMID: 20610736

63. Stitzel SE, Aernecke MJ, Walt DR. Artificial noses. Annu Rev Biomed Eng. 2011; 13:1–25. doi: 10.1146/annurev-bioeng-071910-124633 PMID: 21417721

64. Davison IG, Katz LC. Sparse and selective odor coding by mitral/tufted neurons in the main olfactory bulb. J Neurosci. 2007; 27(8):2091–101. doi: 10.1523/JNEUROSCI.3779-06.2007 PMID: 17314304

65. Rinberg D, Koulakov A, Gelperin A. Sparse odor coding in awake behaving mice. J Neurosci. 2006; 26(34):8857–65. doi: 10.1523/JNEUROSCI.0884-06.2006 PMID: 16928875

66. Perez-Orive J, Mazor O, Turner GC, Cassenaer S, Wilson RI, Laurent G. Oscillations and sparsening of odor representations in the mushroom body. Science. 2002; 297(5580):359–65. doi: 10.1126/science.1070502 PMID: 12130775

67. Lin DY, Zhang SZ, Block E, Katz LC. Encoding social signals in the mouse main olfactory bulb. Nature. 2005; 434(7032):470–7. doi: 10.1038/nature03414 PMID: 15724148

68. Stevens CF. A statistical property of fly odor responses is conserved across odors. Proc Natl Acad Sci USA. 2016; doi: 10.1073/pnas.1606339113 PMID: 27247407

69. Weiss T, Snitz K, Yablonka A, Khan RM, Gafsou D, Schneidman E, et al. Perceptual convergence of multi-component mixtures in olfaction implies an olfactory white. Proc Natl Acad Sci USA. 2012; 109(49):19959–19964. doi: 10.1073/pnas.1208110109 PMID: 23169632

70. Bushdid C, Magnasco M, Vosshall L, Keller A. Humans can discriminate more than 1 trillion olfactory stimuli. Science. 2014; 343(6177):1370–1372. doi: 10.1126/science.1249168 PMID: 24653035

71. Lazarini F, Lledo PM. Is adult neurogenesis essential for olfaction? Trends Neurosci. 2011; 34(1):20–30. doi: 10.1016/j.tins.2010.09.006 PMID: 20980064

72. Pelosi P. The role of perireceptor events in vertebrate olfaction. Cellular and Molecular Life Sciences CMLS. 2001; 58(4):503–509. doi: 10.1007/PL00000875 PMID: 11361085

73. Schoenfeld TA, Cleland TA. The anatomical logic of smell. Trends in neurosciences. 2005; 28(11):620–627. doi: 10.1016/j.tins.2005.09.005 PMID: 16182387

74. Mathis A, Rokni D, Kapoor V, Bethge M, Murthy VN. Reading out olfactory receptors: feedforward circuits detect odors in mixtures without demixing. bioRxiv. 2016; p. 054247.

75. Ukhanov K, Corey EA, Brunert D, Klasen K, Ache BW. Inhibitory odorant signaling in Mammalian olfactory receptor neurons. J Neurophysiol. 2010; 103(2):1114–22. doi: 10.1152/jn.00980.2009 PMID: 20032232

76. Arevian AC, Kapoor V, Urban NN. Activity-dependent gating of lateral inhibition in the mouse olfactory bulb. Nat Neurosci. 2008; 11(1):80–7. doi: 10.1038/nn2030 PMID: 18084286

77. Wilson RI. Understanding the functional consequences of synaptic specialization: insight from the Drosophila antennal lobe. Curr Opin Neurobiol. 2011; 21(2):254–60. doi: 10.1016/j.conb.2011.03.002 PMID: 21441021

78. Leon M, Johnson BA. Olfactory coding in the mammalian olfactory bulb. Brain Res Rev. 2003; 42(1):23–32. doi: 10.1016/S0165-0173(03)00142-5 PMID: 12668289

79. Geramita MA, Burton SD, Urban NN. Distinct lateral inhibitory circuits drive parallel processing of sensory information in the mammalian olfactory bulb. Elife. 2016; 5. doi: 10.7554/eLife.16039 PMID: 27351103

80. Zufall F, Leinders-Zufall T. The cellular and molecular basis of odor adaptation. Chem Senses. 2000; 25(4):473–81. doi: 10.1093/chemse/25.4.473 PMID: 10944513

81. Sirotin YB, Shusterman R, Rinberg D. Neural Coding of Perceived Odor Intensity. eNeuro. 2015; 2(6). doi: 10.1523/ENEURO.0083-15.2015 PMID: 26665162

82. Gupta P, Albeanu DF, Bhalla US. Olfactory bulb coding of odors, mixtures and sniffs is a linear sum of odor time profiles. Nat Neurosci. 2015; 18(2):272–81. doi: 10.1038/nn.3913 PMID: 25581362

83. Uchida N, Poo C, Haddad R. Coding and transformations in the olfactory system. Annu Rev Neurosci. 2014; 37:363–85. doi: 10.1146/annurev-neuro-071013-013941 PMID: 24905594

84. Blauvelt DG, Sato TF, Wienisch M, Murthy VN. Distinct spatiotemporal activity in principal neurons of the mouse olfactory bulb in anesthetized and awake states. Frontiers in neural circuits. 2013; 7(46). doi: 10.3389/fncir.2013.00046 PMID: 23543674